

1     **Carbonate clumped isotope evidence for latitudinal seawater temperature gradients and the**  
2                                   **oxygen isotope composition of Early Cretaceous seas**

3

4                                   Gregory D. Price<sup>1\*</sup>, David Bajnai<sup>2,3</sup>, Jens Fiebig<sup>2</sup>

5

6     <sup>1</sup> School of Geography, Earth & Environmental Sciences, University of Plymouth, Drake Circus,  
7     PL4 8AA Plymouth, UK

8     <sup>2</sup> Institute of Geosciences, Goethe University Frankfurt, Altenhöferallee 1, 60438 Frankfurt am  
9     Main, Germany

10    <sup>3</sup> Institute of Geology and Mineralogy, University of Cologne, Zùlpicher Str. 49b, 50674 Cologne,  
11    Germany

12    \*Corresponding author, email: [g.price@plymouth.ac.uk](mailto:g.price@plymouth.ac.uk), phone: +44 1752 584771

13

14    **Keywords:** thermometry, Valanginian, stable isotopes, belemnites

15 **Abstract**

16           In this study, we investigated Early Cretaceous (Valanginian, ca. 135 million years ago)  
17 climate from subtropical to boreal palaeolatitudes. Combined carbonate clumped isotope and  
18 oxygen isotope data derived from sub-arctic, boreal, and sub-tropical fossil belemnite rostra  
19 (Mollusca: Cephalopoda) provide new palaeotemperature estimates as well as a constraint on  
20 the oxygen isotope composition of seawater. Our belemnite data reveal balmy high-latitude  
21 marine temperatures (ca. 22 °C) and warm sub-tropical temperatures (ca. 31 °C).  
22 Supplementing our clumped isotope-based temperature estimates with published TEX<sub>86</sub> data  
23 results in a conservative reconstruction of a latitudinal temperature gradient that is reduced  
24 compared to modern conditions. We find that modelling efforts are close to reproducing  
25 tropical temperatures when high  $p\text{CO}_2$  levels are considered. Warm polar temperatures imply,  
26 however, that data-model discrepancies remain. Early Cretaceous seawater oxygen isotope  
27 values show a modern profile and are much more positive (up to 1.5‰ SMOW) than typically  
28 assumed. Based on our findings, if the positive Cretaceous seawater  $\delta^{18}\text{O}$  values are not  
29 considered, carbonate  $\delta^{18}\text{O}$  thermometry would underestimate temperatures, most acute at  
30 middle and tropical latitudes.

## 31        **1    Introduction**

32            Existing proxy data suggest that the Cretaceous latitudinal sea-surface temperature  
33 (SST) gradient was reduced (Barron, 1983; Naafs and Pancost, 2016; Littler et al., 2011; Voigt et  
34 al., 2003; Pucéat et al., 2003). The presence of extensive polar ice at this time, as suggested by  
35 Miller (2009) for example, is at odds with contemporaneous warm polar ocean temperatures,  
36 variable but high atmospheric CO<sub>2</sub> level (Bernier and Kothavala, 2001; Wang et al., 2014;  
37 Witkowski et al., 2018) and the occurrence of tropical flora at mid- to high latitudes (Grasby et  
38 al., 2017). During much of the Cretaceous, stable oxygen isotope and TEX<sub>86</sub> evidence suggests  
39 that equatorial surface waters were warmer (ca. 30–40 °C) and greater than the maximum SSTs  
40 recorded in the modern ocean (e.g. O'Brien et al., 2017; Huber et al., 2018). Mid to higher  
41 latitude surface waters were also 10–20 °C warmer than today (Naafs and Pancost, 2016; Littler  
42 et al., 2011; O'Brien et al., 2017; Huber et al., 1995; Jenkyns et al., 2012; Vickers et al., 2019;  
43 O'Connor et al., 2019).

44            The stable oxygen isotope composition ( $\delta^{18}\text{O}$ ) of skeletal marine carbonates is perhaps  
45 the most widely used palaeotemperature proxy (Barron, 1983; Voigt et al., 2003; Pucéat et al.,  
46 2003; Huber et al., 2018; Mutterlose et al., 2012; Price et al., 2018). The challenge is, however,  
47 that the oxygen isotope composition of skeletal carbonates in marine systems vary as a  
48 function of both ambient temperatures and the oxygen isotope composition of seawater  
49 ( $\delta^{18}\text{O}_{\text{sw}}$ ). Obtaining a value for  $\delta^{18}\text{O}_{\text{sw}}$  is complicated because of variables that cannot be easily  
50 independently quantified, such as freshwater input, evaporation, and the extent of polar ice  
51 (Frakes and Francis, 1988; Price, 1999; Miller, 2009; Wierzbowski et al., 2018). Additionally, a  
52 proposed change in the mode of mid-ocean ridge hydrothermal alteration over tens of million  
53 year timescales suggests that the  $\delta^{18}\text{O}_{\text{sw}}$  value has increased gradually through Earth's history,  
54 from ca. -6‰ SMOW in the Cambrian to its present value of ca. 0‰ SMOW (Standard Mean  
55 Ocean Water) (Veizer and Prokoph, 2015; Jaffrés et al., 2007). Nevertheless, the implied

56 climatic warmth, derived from the  $\delta^{18}\text{O}$  values of skeletal marine carbonates, is consistent with  
57 more qualitative data derived from thermophilic floras and faunas from the high latitudes  
58 (Frakes and Francis, 1988; Tarduno, et al., 1998; Hurum et al., 2006; Spicer et al., 2008; Spicer  
59 and Herman 2010). However, Cretaceous General Circulation Model (GCM) simulations indicate  
60 that the latitudinal temperature gradient was much steeper than what the geological record  
61 suggests (Donnadieu et al., 2016; Lunt et al., 2016; Zhou et al., 2008; Poulsen et al., 2007).

62 The clumped isotope palaeothermometry technique measures the abundance of heavy  
63 ( $^{13}\text{C}$ – $^{18}\text{O}$  bond bearing, mass 47) carbonate isotopologues within the single carbonate phase  
64 relative to its stochastic distribution, which is expressed as the  $\Delta_{47}$  value. Clumped isotope-  
65 derived seawater temperatures are independent of the oxygen isotope composition of the  
66 waters (Ghosh et al., 2006). In this study, we analyse belemnite rostra (fossil remains of extinct  
67 marine cephalopods) using clumped isotope thermometry to provide new  $\Delta_{47}$  data from the  
68 Early Cretaceous (Valanginian). Further, we examine equator-to-pole seawater temperature  
69 gradients and the  $\delta^{18}\text{O}_{\text{sw}}$  values to aid temperature reconstructions and palaeoclimate  
70 modelling efforts.

71

## 72 **2 Materials and methods**

### 73 *2.1 Stratigraphic and environmental setting*

74 Belemnite rostra for this study were collected from four locations: the Khatanga Basin  
75 (Boyarka River, Russia, 70.592611° N, 97.369083° E), the Pechora Basin (Izhma River, Russia,  
76 64.835150° N, 53.782200° E), the Cleveland Basin (Speeton, UK, 54.160555° N, 0.236111° W),  
77 and Caravaca (Southern Spain, 38.086944° N, 1.853889° W). These sites are spread across  
78 Tethyan, sub-Boreal, and Boreal locations, with palaeolatitudes ranging from 24° N to 74° N  
79 (Fig. 1).

80           The Lower Cretaceous part of the Boyarka River section is ca. 300 m thick and consists  
81 of marine sandstones, siltstones, and clays deposited in water depths of less than 100 m (Nunn  
82 et al., 2010). The fully marine macrofauna includes belemnites and ammonites, allowing a  
83 detailed Valanginian biostratigraphic zonation consistent with the Boreal biostratigraphic  
84 schemes (Fig. 2) and correlatable to Tethyan ammonite biostratigraphy (Nunn et al., 2010;  
85 Shulgina et al., 1994; Zakharov et al., 1997). Burial-history analysis of the Boyarka River region  
86 of the Khatanga Basin, suggests that a maximum burial depth is likely to be ca. 500 m and  
87 geothermal gradients to be moderate ca. 40 °C/km (Klett et al., 2011; Dobretsov et al., 2013).

88           The ca. 62-m-thick Izhma River section comprises shallow marine clastics with  
89 belemnites and ammonites present throughout. A detailed Berriasian (Ryazanian) to  
90 Valanginian biostratigraphic zonation is consistent with the Boreal biostratigraphic schemes  
91 and correlatable to Tethyan ammonite biostratigraphy (Nunn et al., 2010; Baraboshkin, 2004;  
92 Zakharov et al., 1997). Burial history curves suggest that the burial depth is likely to be no more  
93 than 1000 m, and the present thermal gradients in the Pechora Basin are moderate ca. 19–  
94 35 °C/km (Lindquist, 1999).

95           The Lower Cretaceous successions located near Caravaca, Southern Spain (Mai Valera,  
96 Sierra de Quipar, Canada Luenga) consist of nodular limestones with abundant marine fossils,  
97 including crinoid fragments, overlain by hemipelagic marl-limestone alternations (Aguado et al.,  
98 2000). The successions are thought to have been deposited in a low-energy marine basinal  
99 setting, with an estimated water depth of a few hundreds of meters (Company and Tavera,  
100 2015). Here, the macrofauna consists mainly of belemnites and well-preserved ammonites,  
101 allowing detailed biostratigraphic zonation and correlation of the sections (Aguado et al., 2000;  
102 Janssen, 2003; Company and Tavera, 2015; Price, et al., 2018). The maturity of the organic  
103 matter in these Subbetic sections and other diagenetic observations imply that the burial depth

104 was no more than 1000 m and that the sediments never reached more than 80 °C (Reicherter  
105 et al., 1996).

106           The Speeton Clay Formation of the Cleveland Basin comprises about 100 m of  
107 interbedded shallow marine claystones deposited in water depths of less than 100 m. The  
108 stratigraphical succession contains abundant belemnite rostra and well-preserved ammonites,  
109 allowing detailed biostratigraphy (Rawson, 1973; McArthur et al., 2004) and correlation to  
110 Boreal and Tethyan zonation schemes (Fig. 2). Measured  $^{87}\text{Sr}/^{86}\text{Sr}$  values (McArthur et al., 2004)  
111 show a good agreement between the biostratigraphic data. Vitrinite reflectance data collected  
112 and analysed by Hemingway and Riddler (1982) for the Middle Jurassic, which lies beneath the  
113 Speeton Clay Formation provides a temperature value of 95 °C for these Jurassic rocks. Holliday  
114 (1999) took this information and assuming an average thermal conductivity provided a  
115 geothermal gradient of approximately 30 °C/km and estimated maximum burial depths of ca.  
116 2000 m. For the Cretaceous, the estimated sediment surface temperature used was 20 °C  
117 (Holliday, 1999). These temperature estimates are consistent with the thermal history model  
118 presented by Słowakiewicz et al. (2015) that suggests that the maximum temperatures for the  
119 Lower Cretaceous succession reached ca. 40–50 °C during the early Cenozoic.

120           Theoretical calculations based on laboratory experiments evidence that solid-state  
121 diffusion, even in wet and high-pressure conditions, is insignificant below 100 °C burial  
122 temperatures on a timescale of 135 million years (Passey and Henkes 2012; Brenner et al.,  
123 2018). Thus, the belemnite rostra analysed from these four sections should not have been  
124 affected by solid-state reordering.

125

## 126           2.2 *Sample selection*

127           Belemnite rostra consist of diagenetically stable low-Mg calcite (Saelen, 1989). The  
128 rostra selected for analysis in this study were those deemed to be the best-preserved samples

129 in the previous studies of McArthur et al. (2004), Nunn et al. (2010), Price et al. (2000), and  
130 Price et al. (2018). The excellent preservation of the analysed material is indicated by trace  
131 element concentrations and petrographic analyses, including cathodoluminescence. Diagenetic  
132 alteration of marine calcites often leads to significant enrichments in Mn and Fe (Veizer, 1974).  
133 Diagenetic Mn<sup>2+</sup> ions are also an activator of orange cathodoluminescence in calcites, which is  
134 indicative of the alteration under reducing conditions (Marshall, 1992). All the belemnites  
135 analysed for clumped isotopes, in this study, had low concentrations of Fe (< 120 ppm) and Mn  
136 (< 25 ppm) indicative of good sample preservation (e.g. McArthur et al., 2007; Mutterlose et al.,  
137 2012). These 20 Valanginian belemnite rostra were: *Acroteuthis* sp. from Speeton from the  
138 Polyptychites Ammonite zone; *Berriasibelus*, *Hibolithes* and *Duvalia* from Caravaca from the  
139 Pertransiens–Verrucosum Ammonite zones; *Acroteuthis* and *Pachyteuthis* from Pechora Basin  
140 from the Klimovskiensis to Michalskii Ammonite zones, and *Acroteuthis*, *Lagonibelus* and  
141 *Pachyteuthis* from Khatanga Basin from the Klimovskiensis to Michalskii Ammonite zones  
142 schemes (Fig. 2). Calcite subsamples (ca. 50 mg carbonate powder) were taken from previously  
143 investigated rostra (see above), re-sampled across multiple growth bands, in order to get a  
144 representative amount for clumped isotope analysis. During sampling the belemnite rostra  
145 margins and calcite around the apical zones were avoided, as diagenetic alteration is typically  
146 observed in these parts. Visual inspection also showed belemnite rostra preservation to be  
147 excellent with all specimen displaying honey coloured translucent calcite. This is consistent with  
148 petrographic and cathodoluminescence observations (e.g. non-luminescent rostra) made in  
149 previous research (McArthur et al., 2004; Nunn et al., 2010; Price et al., 2000, 2018).

150

### 151 2.3 Clumped and stable isotope analyses

152 Clumped isotope analyses were performed using a ThermoFisher MAT 253 gas-source  
153 isotope-ratio mass spectrometer connected to an automated gas extraction and purification

154 line at the Institute of Geosciences, Goethe University Frankfurt. Carbonates were digested at  
155 90 °C in a common acid bath. Background correction for the clumped isotope analyses was  
156 performed as described in Fiebig et al. (2016). Raw isotope values were calculated using the  
157 [Brand]/IUPAC set of isotopic parameters as suggested by Daëron et al. (2016). The raw  $\Delta_{47}$   
158 data were projected to the carbon dioxide equilibrium scale using empirical transfer functions  
159 that were determined using equilibrated gases (25 °C and 1000 °C, respectively) of various bulk  
160 isotope composition (Petersen et al., 2019). A 90–25 °C acid fractionation factor of 0.088‰ was  
161 applied to all  $\Delta_{47(RFAC)}$  values (Petersen et al., 2019). To verify the consistency and precision of  
162 the clumped isotope measurements six carbonate standards were independently analysed  
163 along with the samples. The  $\Delta_{47(RFAC)}$  (1 standard deviation, N = number of replicates) values of  
164 the reference material are: Carrara 0.407‰ (0.019‰, N = 335), MuStd 0.749‰ (0.018‰, N =  
165 181), ETH 1 0.301‰ (0.016‰, N = 78), ETH 2 0.301‰ (0.019‰, N = 37), ETH 3 0.711‰  
166 (0.018‰, N = 92), ETH 4 0.556‰ (0.020‰, N = 10) (Data S1). To convert  $\Delta_{47(RFAC)}$  values to  
167 temperatures, we used a synthetic calcite calibration:  $\Delta_{47(RFAC)} = 0.0383(\pm 1.7E-06) \times 10^6/T^2 +$   
168  $0.258(\pm 1.7E-05)$  (Petersen et al., 2019), where  $T$  is in K and  $\Delta_{47(RFAC)}$  is in ‰.  $\delta^{18}O_{sw}$  estimates  
169 (Table 1, Data S1) were calculated using the  $\Delta_{47}$ -derived temperature, the measured  $\delta^{18}O$  value  
170 of each belemnite, and the  $1000 \ln \alpha_{\text{calcite-water-temperature}}$  relationships of Kim and O’Neil  
171 (1997) (corrected for a CO<sub>2</sub>-calcite acid fractionation factor of 10.25, Kim et al. (2007)) and of  
172 Coplen (2007). Coplen (2007) provided an equation based on water and vein calcite  
173 precipitated at extreme slow rates subaqueously at Devils Hole, Nevada, USA. The widely  
174 accepted Kim and O’Neil (1997) equation is based on inorganic precipitation experiments.

175

## 176 **3 Results**

### 177 *3.1 Belemnite $\Delta_{47}$ -based temperatures*



178           The average  $\Delta_{47}$ -derived temperatures of this study range from 19 °C to 27 °C (Fig. 3,  
179 Table 2, Supplementary Figure 1, Data S1). Some studies have postulated that belemnites  
180 calcified their rostra, possibly seasonally, in the upper part of the water column (Klug et al.,  
181 2016; Price et al., 2015; Stevens et al., 2014), whereas others consider belemnites as  
182 nektobenthic organisms (Wierzbowski et al., 2013). For shallow marine settings (i.e. typically  
183 less than 100 m), comparable to the locations investigated in this study (see above), one could  
184 assume a low temperature gradient in the water column. Thus, here we presume that  
185 belemnites indicate mean seawater temperatures at these sites at the time of rostra growth.  
186 The range of  $\Delta_{47}$ -derived temperatures encountered at each of the individual sample site was  
187 from 4 °C to 15 °C. This relatively large temperature range is similar to that seen in other  
188 clumped isotope studies (e.g. Petersen et al., 2016; Evans et al., 2018; Meyer et al., 2018). Such  
189 a range in the  $\Delta_{47}$ -derived temperature data is of a similar magnitude as the modern  
190 temperature range (e.g. 4–12 °C) in similar latitudes (Locarnini et al., 2013) and is attributed to  
191 a combination of the influence of seasonal temperature variability, different belemnite  
192 ecologies combined with the impact of local geography and a reflection of the range of  
193 temperature variability over the timescales represented by the belemnite sample set (see Fig.  
194 2).

195           Our  $\Delta_{47}$ -derived temperature estimate for the Valanginian low latitudes (27 °C) is lower  
196 than the average temperature values of ca. 35 °C obtained from Valanginian  $\text{TEX}_{86}^{\text{H}}$  data (Littler  
197 et al., 2011) but is comparable with modern mean annual surface temperature observations.  
198 Our  $\Delta_{47}$ -based temperatures suggest, therefore, that belemnites were calcifying their rostra in  
199 waters slightly cooler than those surface waters indicated by the  $\text{TEX}_{86}$  data. Notably, the  
200 belemnites from Caravaca occur in hemipelagic marly-limestone beds formed at a depth of a  
201 few hundred meters (see above) and may have lived at times below a thermocline layer, so  
202 their clumped isotope record may be subject to lower temperatures. Vickers et al. (2019) also

203 showed that  $\Delta_{47}$ -derived palaeotemperatures were slightly cooler than  $\text{TEX}_{86}$ -based estimates.  
204 Multiple studies have now found that clumped temperatures of molluscs are always colder  
205 than  $\text{TEX}_{86}$ , temperature estimates, whether using the  $\text{TEX}_{86}^{\text{H}}$  or BAYSPAR  $\text{TEX}_{86}$  calibration. The  
206 temperature difference is commonly too great to be explained by surface vs. benthic modes of  
207 life alone (see Meyers et al., 2018). Despite the relatively large uncertainty in our temperatures  
208 estimates, our average Valanginian temperatures (19–24 °C) for the middle latitudes are  
209 warmer by up to 13 °C than other Valanginian temperature estimates derived from  $\delta^{18}\text{O}$   
210 thermometry of belemnites (Schootbrugge et al., 2000; Price et al., 2000; McArthur et al.,  
211 2004), although similar to Pucéat et al. (2003), who inferred temperatures from the oxygen  
212 isotope composition of fish tooth enamels. Our average Valanginian temperatures are also  
213 comparable to  $\text{TEX}_{86}^{\text{H}}$  data from other Cretaceous intervals (Mutterlose et al., 2010, 2012;  
214 Naafs and Pancost, 2016; O'Brien et al., 2017). For example, Mutterlose et al. (2012) suggest  
215  $\text{TEX}_{86}^{\text{H}}$  seawater temperature estimates ranging from 22 °C to 24 °C for the Hauterivian of  
216 Speeton, UK. The temperature estimate for higher paleolatitudes (74° N) from this study is  
217 19 °C and is warmer than previous Valanginian carbonate  $\delta^{18}\text{O}$ -based estimates (Price and  
218 Nunn, 2010; Ditchfield, 1997) but similar to Late Cretaceous  $\text{TEX}_{86}^{\text{H}}$  seawater temperature  
219 estimates (Super et al., 2018). Different calibrations have been proposed to translate  $\text{TEX}_{86}$  into  
220 SST. Of these calibrations, the global nonlinear logarithmic  $\text{TEX}_{86}^{\text{H}}$  calibration of Kim et al.  
221 (2010) and the BAYSPAR  $\text{TEX}_{86}$  calibration of Tierney and Tingley (2014) are the most commonly  
222 chosen for higher-temperature settings, such as in the Cretaceous. It is the more conservative  
223  $\text{TEX}_{86}^{\text{H}}$  estimates that provide a better match to our clumped isotope temperature estimates  
224 (see also Vickers et al., 2019). The BAYSPAR  $\text{TEX}_{86}$  calibration of Tierney and Tingley (2014)  
225 provides higher temperatures (ca. 8 °C higher) at the upper limit of the proxy (e.g. O'Brien et al.  
226 2017; O'Connor et al., 2019). Our Valanginian seawater temperatures across all latitudes are

227 also 1–14 °C warmer than modern SST observations, although at middle latitudes, they  
228 approach the warmest recent observations (Locarnini et al., 2013).

229         The interpretation of relatively warm past ocean temperatures at middle-high latitudes  
230 is consistent with palaeobotanical temperature constraints derived from Cretaceous fossil  
231 floras (Spicer and Herman, 2010). In contrast, data from the Lower Cretaceous of Canada  
232 (Grasby et al., 2017), Svalbard (Vickers et al., 2016), and Siberia (Rogov et al., 2017) suggest that  
233 numerous boreal cool events interrupted otherwise warm conditions. These authors describe  
234 abundant glendonites (pseudomorphs after marine sedimentary ikaite) in Valanginian and  
235 Aptian strata that are thought to be critical markers of cold conditions. These observations are  
236 not incompatible with our data from the Valanginian, as Grasby et al. (2017) conclude that cold  
237 periods were brief, punctuating an overall warm Early Cretaceous climate.

238

## 239         **4 Discussion**

### 240             *4.1 Early Cretaceous latitudinal temperature gradient*

241         Using the average palaeotemperatures and the palaeolatitude (Young et al., 2019) at  
242 each of the sites examined here, together with Valanginian  $\Delta_{47}$  data from Price and Passey  
243 (2013) and TEX<sub>86</sub> data from Littler et al. (2011), we can conservatively reconstruct an Early  
244 Cretaceous latitudinal temperature profile with an estimated gradient of ca. 0.32 °C per degree  
245 of latitude, between 15° N and 74° N (Fig. 3). TEX<sub>86</sub> data from other Early Cretaceous intervals  
246 (Naafs and Pancost, 2016) and Late Cretaceous  $\delta^{18}\text{O}$ -derived palaeotemperatures (Voigt et al.,  
247 2003; Pucéat et al., 2003) also reveal a similar gradient. Available TEX<sub>86</sub> data evidence (O’Brien  
248 et al. 2017; O’Connor et al., 2019) suggests that latitudinal temperature gradients were lower in  
249 the Coniacian to Campanian compared with the present day. The implied shallow meridional  
250 temperature gradient for the Early Cretaceous contrasts with a modern average gradient of ca.  
251 0.45 °C per degree of latitude in the Northern Hemisphere (Young et al., 2019).

252 Most evidence suggests that the Cretaceous was characterised by high atmospheric CO<sub>2</sub>  
253 levels (e.g. Berner and Kothavala, 2001; Wang et al., 2014; Witkowski et al., 2018) and  
254 consequently, its climate was warmer and more equable (Frakes 1979; Huber et al., 1995; Bice  
255 et al., 2003). Although, as noted above, transient cool events have been suggested (Grasby et  
256 al., 2017; Mutterlose et al., 2010; McArthur et al., 2007), data typically point to warm polar  
257 regions (Spicer and Herman, 2010; Ditchfield 1997; Frakes, 1979; McArthur et al., 2007)  
258 consistent with our temperature estimates. The presence of such a reduced temperature  
259 gradient requires a climate mechanism in a high *p*CO<sub>2</sub>-world that yields temperate polar regions  
260 while not overheating the tropics. Proposed mechanisms to increase the transfer of heat  
261 toward the poles include increased oceanic (Schmidt and Mysak, 1996) and atmospheric  
262 poleward heat transport (Bice et al., 2003), together with amplification of polar warmth by  
263 cloud feedbacks (Kump and Pollard 2008; Sagoo et al., 2013; Upchurch et al., 2015).

264

#### 265 4.2 *Cretaceous model-data comparisons*

266 Climate modelling of past warm periods has received much attention as it has long been  
267 suggested that simulations may not capture the extent to which the latitudinal temperature  
268 gradient is reduced (Spicer, et al., 2008). The  $\Delta_{47}$  reconstructions and temperature compilation  
269 demonstrate that Early Cretaceous tropical warming was of a magnitude consistent with some  
270 models (e.g. using the fast ocean atmosphere model (FOAM), for the Late Cretaceous,  
271 Donnadieu et al., 2016) at 12-times pre-industrial *p*CO<sub>2</sub> (Fig. 3). Other simulations indicate  
272 cooler tropical temperatures. For example, modelled Valanginian sea surface temperatures  
273 (using the UK Met Office HadCM3L model) with 4x pre-industrial *p*CO<sub>2</sub> (Lunt et al., 2016) shows  
274 less of a fit particularly with the Littler et al. (2011) TEX<sub>86</sub> temperature data, which represents  
275 the sea surface, as does the model. For higher latitudes, our temperature proxy data are  
276 warmer than some simulations (Donnadieu et al., 2016; Lunt et al., 2016; Poulsen et al., 2007;

277 Upchurch et al., 2015) for the Early and Late Cretaceous even at 12-times pre-industrial  $p\text{CO}_2$ .  
278 In contrast to these Cretaceous simulations, climate models of other “greenhouse” intervals  
279 (e.g. for the Eocene, Sagoo et al., 2013; Zhu et al., 2019), show warmer higher latitudes.  
280 Although many aspects contributed to the warmth seen at higher latitudes in the model of  
281 Sagoo et al., (2013), a strong sensitivity to albedo changes associated with cloud cover was  
282 apparent. However, for the highest latitude proxy data, the magnitude of warming simulated  
283 by most climate models is still less than indicated by the  $\Delta_{47}$  data and published  $\text{TEX}_{86}$  (Jenkyns  
284 et al., 2012) temperature estimates. This could suggest that some climate models for the  
285 Cretaceous are still missing key processes. Notably, Upchurch et al. (2015) using a fully coupled  
286 GCM come close to reproduce warm Cretaceous polar temperatures and the latitudinal  
287 temperature gradient without overheating the tropics. For a cool greenhouse interval of the  
288 latest Cretaceous (Maastrichtian) the best fits of Upchurch et al. (2015) for mean annual  
289 temperature are simulations that use 6-times pre-industrial levels of atmospheric  $\text{CO}_2$ , or 2-  
290 times pre-industrial levels of atmospheric  $\text{CO}_2$  and liquid cloud properties that may reflect pre-  
291 anthropogenic levels of cloud condensation nuclei. It is important to note that Cretaceous  $\text{TEX}_{86}$   
292 data and  $\Delta_{47}$ -derived temperatures are limited by the distribution of suitably preserved  
293 sediments at high latitudes. Indeed, Cretaceous  $\text{TEX}_{86}$  data is available from just a few Arctic  
294 sites (Jenkyns et al., 2004; Super et al., 2018). As such, the high temperatures so far identified  
295 may not be fully representative of regional averages.

296

#### 297 4.3 *The oxygen isotope composition of Early Cretaceous seas*

298 Estimations of ancient oceans  $\delta^{18}\text{O}_{\text{sw}}$  values are controversial. Complexity arises from  
299 variables such as the input of freshwater and evaporation, the presence or absence of polar ice,  
300 whether the oxygen isotope composition of the seawater is buffered by submarine  
301 hydrothermal processes, or whether lower  $\delta^{18}\text{O}$  values of ancient marine carbonates reflect the

302 fact that the  $\delta^{18}\text{O}_{\text{sw}}$  value has varied significantly over time (see Jaffrés et al., 2007). The  
303 average of our  $\delta^{18}\text{O}_{\text{sw}}$  estimates is calculated as -0.1‰ SMOW using the Coplen (2007) equation  
304 or 1.4‰ SMOW using the Kim and O’Neil (1997) equation (Table 2, Data S1). Both values are  
305 more positive than the estimated global average  $\delta^{18}\text{O}_{\text{sw}}$  value for the modern ocean (-0.28‰  
306 SMOW) or an ice-free world (-1.0‰ SMOW) (Shackleton and Kennett, 1975) (Fig. 4). The  $\delta^{18}\text{O}_{\text{sw}}$   
307 value of -1.0‰ SMOW is widely cited as the mean seawater oxygen isotope composition for the  
308 Cretaceous. Nevertheless, our data from four new sites, in conjunction with data from Price  
309 and Passey (2013), suggests a gentle decrease in average values poleward (Fig. 4,  
310 Supplementary Figure 2) (see also Zhou et al., 2008). The difference between our calculated  
311  $\delta^{18}\text{O}_{\text{sw}}$  values and modern  $\delta^{18}\text{O}_{\text{sw}}$  values, or the assumed  $\delta^{18}\text{O}_{\text{sw}}$  values for ancient seas in ice-  
312 free hothouse worlds, may be due to (1) differences in the absolute  $\Delta_{47}$ -temperature calibration  
313 producing temperatures that are too warm, (2) vital effects in the belemnites resulting in  
314 carbonate  $\delta^{18}\text{O}$  values enriched relative to equilibrium with seawater, (3) diagenesis causing  
315 lower  $\Delta_{47}$  and higher  $\delta^{18}\text{O}$  values in carbonates, or (4) changes in  $\delta^{18}\text{O}_{\text{sw}}$  values of ancient seas.

316 Differences in the  $\Delta_{47}$ -temperature calibration would influence absolute temperature  
317 and calculated  $\delta^{18}\text{O}_{\text{sw}}$  values. As noted above, we used the synthetic  $\Delta_{47}$ -temperature  
318 calibration of Petersen et al. (2019) to convert the measured clumped isotope values to  
319 precipitation temperatures of calcium carbonate. This calibration is fairly robust as it considers  
320 451 carbonate datapoints. In comparison, the in-house Wacker et al. (2014) or the steeper  
321 sloped Kelson et al. (2017) calibrations give temperatures that are ca. 3 °C warmer (Data S1).  
322 Hence our choice of calibration eliminates potential biasing towards too warm temperatures.

323 Alternatively, the high  $\delta^{18}\text{O}_{\text{sw}}$  values could be caused by diagenetic effects that  
324 increased temperatures. Modelling of burial at all sites suggests that the belemnite rostra  
325 analysed should not have been affected by solid-state reordering. Alternatively, the high  $\delta^{18}\text{O}_{\text{sw}}$   
326 values may be due to vital effects. Should Kim and O’Neil (1997) represent equilibrium, then

327 our mean  $\delta^{18}\text{O}_{\text{sw}}$  value would be on average 2.4‰ higher than the value assumed for an ice-  
328 free ocean (see below). Kinetic isotope effects generally, however, discriminate against the  
329 heavier isotope (e.g. McConnaughey 1989), although Price et al. (2015) do suggest a possible  
330 offset between belemnite calcite  $\delta^{18}\text{O}$  and equilibrium of ca. 1‰. Data from a number of other  
331 Cretaceous studies applying the clumped isotope palaeothermometer to molluscs (Dennis et  
332 al., 2013; Meyer et al., 2018; Vickers et al., 2019), also indicates that the isotopic composition  
333 of seawater predicted was markedly positive, using the equation of Kim and O'Neil (1997) and  
334 exceeding modern seawater values. Further work comparing the clumped isotope  
335 temperatures to different molluscs (see Meyer et al. 2018) could resolve whether these high  
336  $\delta^{18}\text{O}_{\text{sw}}$  values could be caused by vital effects.

337 In addition to those studies noted above, data from a number of other studies applying  
338 the clumped isotope palaeothermometer (Petersen and Schrag 2015; Wierzbowski et al 2018),  
339 also note that the isotopic composition of seawater predicted was, at times, markedly positive.  
340 This poses a challenge, as the average value of modern  $\delta^{18}\text{O}_{\text{sw}}$  is a consequence of ice  
341 accumulation largely on Greenland and Antarctica. Although modest-sized Cretaceous ice  
342 sheets have been postulated (DeConto and Pollard, 2003; Frakes and Francis, 1988; Price,  
343 1999), the volume of this ice is likely to be insufficient to see  $\delta^{18}\text{O}_{\text{sw}}$  values around 1‰ SMOW.  
344  $\delta^{18}\text{O}_{\text{sw}}$  values of 1‰ SMOW require ice volumes in excess of the Last Glacial Maximum, when  
345 ice sheets covered large parts of North America and Europe as well as Antarctica. Unlike at the  
346 Last Glacial Maximum, it is thought that in the Cretaceous, ice was considerably more limited  
347 and is, therefore, not sufficient to explain such high  $\delta^{18}\text{O}_{\text{sw}}$  values. Any ice would also have to  
348 be isotopically very light. Studies have also postulated that water could be stored as  
349 (isotopically light) freshwater on land (e.g. Jacobs and Sahagian, 1993). As this study, however,  
350 suggests that the latitudinal temperature gradient during the Early Cretaceous was less steep  
351 than today, it is conceivable that the  $\delta^{18}\text{O}_{\text{ice}}$  and any stored freshwater was also less extreme. If

352 the  $\delta^{18}\text{O}_{\text{ice}}$  value was less negative, this would make it even harder to get  $\delta^{18}\text{O}_{\text{sw}}$  values to 1‰  
353 SMOW or more, as even greater ice volumes would be required. This is consistent with studies  
354 of the Antarctic ice sheet during the early Miocene when the latitudinal temperature gradient  
355 was less extreme and Antarctic temperatures were warmer than today resulting in significantly  
356 higher  $\delta^{18}\text{O}_{\text{ice}}$  values in the Miocene ice sheet (e.g. ca. -35‰ SMOW) than values today  
357 (i.e. -45‰ to -55‰ SMOW) (Pekar and DeConto, 2006).

358         Alternatively, the high  $\delta^{18}\text{O}_{\text{sw}}$  values could be caused by relatively high rates of  
359 evaporation leading to higher salinities. Although, salinity can be estimated from salinity– $\delta^{18}\text{O}$   
360 models for marine basins (e.g. Railsback et al., 1989), to reconcile our belemnite  $\delta^{18}\text{O}$  data with  
361 the  $\Delta_{47}$ -derived temperatures, salinities in excess of 41 PSU are required (see also Wierzbowski  
362 et al., 2018). As such, each of the sites examined here would need to be dominated by  
363 evaporation. As the belemnite samples were derived from open marine systems (based upon  
364 the presence of a fully marine fauna, including ammonites), high salinities contributing to high  
365  $\delta^{18}\text{O}_{\text{sw}}$  values seems unlikely.

366         The marine carbonate  $\delta^{18}\text{O}$  record also depends on seawater pH (Wallmann, 2004).  
367 Seawater pH is strongly influenced by changes in  $p\text{CO}_2$  (Zeebe, 1999, 2001; Wallmann, 2004).  
368 An increase of seawater pH of 0.2–0.3 units, for example, is considered to result in a decrease  
369 of about 0.22–0.33‰ in the  $\delta^{18}\text{O}$  values of foraminiferal calcite, which would normally be  
370 interpreted as a temperature increase of seawater, although the magnitude of the effect may  
371 be species-dependent (Zeebe, 2001). During periods of high atmospheric  $\text{CO}_2$  levels such as the  
372 Cretaceous (Bernier and Kothavala, 2001; Wang et al., 2014; Witkowski et al., 2018), this pH  
373 effect (Zeebe, 2001) if applicable to belemnites, would lead to an increase in the  $\delta^{18}\text{O}$  value of  
374 calcite. However, the magnitude of pH change in seawater needed to explain the observed  
375 offset in  $\delta^{18}\text{O}_{\text{sw}}$  value between an ice-free -1‰ SMOW and the average of our estimate of  
376 +1.5‰ SMOW (using the Kim and O’Neil, 1997 equation) and scaling of ca. 0.1 pH unit for every



377 0.1‰  $\delta^{18}\text{O}$ , means that oceans would need to be ca. 2.5 pH units more acidic. Such a  
378 magnitude of change is not realistic (see Caldeira and Wickett, 2003).

379 Changes in the oxygen isotope composition of ancient oceans is a debated issue. Veizer  
380 and Prokoph (2015) and Jaffrés et al. (2007) for example suggest that the  $\delta^{18}\text{O}_{\text{sw}}$  value has  
381 increased gradually through Earth's history, from -6‰ SMOW in the Cambrian to its present  
382 value of ca. 0‰ SMOW. Other studies, applying the clumped isotope palaeothermometer,  
383 indicate more or less constant  $\delta^{18}\text{O}_{\text{sw}}$  values through geologic time (e.g. Ryb and Eiler, 2018;  
384 Henkes, et al., 2018). Most models of the geological  $^{18}\text{O}$ -cycle conclude that seawater/rock  
385 interaction with silicates of oceanic crust at high and low temperatures balance each other and,  
386 thus buffer the  $\delta^{18}\text{O}_{\text{sw}}$  value at about  $0(\pm 2)\%$  SMOW (Muehlenbachs and Clayton, 1976;  
387 Holland, 1984). Hence, it has been considered that the  $\delta^{18}\text{O}_{\text{sw}}$  value of the global ocean has not  
388 changed significantly over time, but has been buffered by hydrothermal and weathering  
389 processes (low-temperature interactions with silicates) at mid-ocean ridges and on ridge flanks,  
390 based on results of ophiolite studies (e.g. Coogan et al., 2019). High-temperature alteration  
391 (mainly via hydrothermal fluids) leads to an increase in  $\delta^{18}\text{O}_{\text{sw}}$  values, while low-temperature  
392 alteration (e.g. weathering processes) leave the ocean  $^{18}\text{O}$ -depleted (Muehlenbachs and  
393 Clayton, 1976; Holland, 1984; Muehlenbachs, 1998). These mass balance calculations, however,  
394 do not rule out minor variations in the average  $\delta^{18}\text{O}_{\text{sw}}$  value that could conceivably produce a  
395 minor change towards more positive values reconciling our belemnite  $\delta^{18}\text{O}$  data and  
396 corresponding  $\Delta_{47}$ -derived temperatures.

## 397 **5 Conclusions**

398 The Early Cretaceous  $\Delta_{47}$ -derived temperatures of this study point to Arctic regions  
399 above freezing. Our data argue against an extended ice sheet in the Northern Hemisphere and  
400 shows congruence with  $\text{TEX}_{86}$  temperatures. Our clumped isotope-based temperature  
401 reconstruction suggests the existence of a strongly reduced equator-to-pole temperature

402 gradient in the Northern Hemisphere. We find that modelling efforts are close to reproducing  
403 the tropical temperatures when high atmospheric CO<sub>2</sub> levels are invoked, however, our data  
404 suggests warmer temperatures at higher latitudes that are not shown in the models.

405 The results of this study indicate that it is unlikely that the oxygen isotope composition  
406 of the seawater was homogenous. Our Early Cretaceous  $\delta^{18}\text{O}_{\text{sw}}$  results are a conservative  
407 reconstruction of a latitudinal gradient that shows a gentle decrease in values poleward and  
408 also, using the Kim and O'Neil (1997) and Coplen (2007) equations plot in the upper portion or  
409 wholly within the field of modern seawater. Early Cretaceous  $\delta^{18}\text{O}_{\text{sw}}$  values with modern  
410 characteristics implies some storage of light isotopes away from the ocean, e.g. as ice  
411 accumulation on Antarctica. The constraints we provide on the oxygen isotope composition of  
412 Early Cretaceous seawater, underpins our understanding of the evolution of the Earth's  
413 temperature. Disregarding positive Early Cretaceous  $\delta^{18}\text{O}_{\text{sw}}$  values results in an  
414 underestimation of temperatures, most acute at middle and tropical latitudes.

415

#### 416 **Acknowledgements**

417 Funding for this study was provided by a UK Natural Environment Research Council  
418 (NERC) grant (NE/J020842/1) to GDP. We thank S. Hofmann, C. Schreiber (Goethe University  
419 Frankfurt), N. Löffler, K. Methner and E. Krsnik (Senckenberg BIK-F) for their technical help.  
420 Further supporting data can be accessed in Table 1 of Supporting information. The authors  
421 declare no conflicts of interest. We would like to thank reviewers Sierra Petersen and Hubert  
422 Wierzbowski for comprehensive and constructive reviews that greatly improved the  
423 manuscript. Comments from Thomas Algeo also improved the manuscript. Further supporting  
424 data can be accessed in the Supporting information and on Pangaea  
425 (<https://doi.pangaea.de/10.1594/PANGAEA.907273>)

426

427 **References**

- 428 Aguado, R., Company, M., Tavera, J.M., 2000. The Berriasian/Valanginian boundary in the  
429 Mediterranean region: New data from the Caravaca and Cehegín sections, SE Spain.  
430 *Cretac. Res.* 21, 1-21. <https://doi.org/10.1006/cres.2000.0198>
- 431 Baraboshkin, E.Y., 2004. Boreal-Tethyan correlation of Lower Cretaceous ammonite scales.  
432 *Moscow Univ. Geol. Bull.* 59, 9-20.
- 433 Barron, E.J., 1983. A warm, equable Cretaceous: The nature of the problem. *Earth-Sci. Rev.* 19,  
434 305-338. [https://doi.org/10.1016/0012-8252\(83\)90001-6](https://doi.org/10.1016/0012-8252(83)90001-6)
- 435 Berner, R.A., Kothavala, Z., 2001. GEOCARB III: A revised model of atmospheric CO<sub>2</sub> over  
436 phanerozoic time. *Am. J. Sci.* 301, 182-204. <https://doi.org/10.2475/ajs.301.2.182>
- 437 Bice, K.L., Huber, B.T., Norris, R.D., 2003. Extreme polar warmth during the Cretaceous  
438 greenhouse? Paradox of the late Turonian  $\delta^{18}\text{O}$  record at Deep Sea Drilling Project Site  
439 511. *Paleoceanography* 18, 1031. <https://doi.org/10.1029/2002pa000848>
- 440 Brenner, D.C., Passey, B.H., Stolper, D.A., 2018. Influence of water on clumped-isotope bond  
441 reordering kinetics in calcite. *Geochim. Cosmochim. Acta* 224, 42-63.  
442 <https://doi.org/10.1016/j.gca.2017.12.026>
- 443 Caldeira, K., Wickett, M.E., 2003. Oceanography: Anthropogenic carbon and ocean pH. *Nature*  
444 425, 365. <https://doi.org/10.1038/425365a>
- 445 Company, M., Tavera, J.M., 2015. Lower Valanginian ammonite biostratigraphy in the Subbetic  
446 Domain (Betic Cordillera, southeastern Spain). *Carnets Geol.* 15, 71-88.
- 447 Coogan, L.A., Daëron, M., Gillis, K.M., 2019. Seafloor weathering and the oxygen isotope ratio in  
448 seawater: Insight from whole-rock  $\delta^{18}\text{O}$  and carbonate  $\delta^{18}\text{O}$  and  $\Delta_{47}$  from the Troodos  
449 ophiolite. *Earth Planet. Sci. Lett.* 508, 41-50. <https://doi.org/10.1016/j.epsl.2018.12.014>

450 Coplen, T.B., 2007. Calibration of the calcite–water oxygen-isotope geothermometer at Devils  
451 Hole, Nevada, a natural laboratory. *Geochim. Cosmochim. Acta* 71, 3948-3957.  
452 <https://doi.org/10.1016/j.gca.2007.05.028>

453 Daëron, M., Blamart, D., Peral, M., Affek, H.P., 2016. Absolute isotopic abundance ratios and  
454 the accuracy of  $\Delta_{47}$  measurements. *Chem. Geol.* 442, 83-96.  
455 <https://doi.org/10.1016/j.chemgeo.2016.08.014>

456 DeConto, R.M., Pollard, D., 2003. Rapid Cenozoic glaciation of Antarctica induced by declining  
457 atmospheric CO<sub>2</sub>. *Nature* 421, 245-249. <https://doi.org/10.1038/nature01290>

458 Dennis, K.J., Cochran, J.K., Landman, N.H., Schrag, D.P., 2013. The climate of the Late  
459 Cretaceous: New insights from the application of the carbonate clumped isotope  
460 thermometer to Western Interior Seaway macrofossil. *Earth Planet. Sci. Lett.* 362, 51-65.  
461 <https://doi.org/10.1016/j.epsl.2012.11.036>

462 Ditchfield, P.W., 1997. High northern palaeolatitude Jurassic-Cretaceous palaeotemperature  
463 variation: new data from Kong Karls Land, Svalbard. *Palaeogeogr. Palaeoclimatol.*  
464 *Palaeoecol.* 130, 163-175. [https://doi.org/10.1016/S0031-0182\(96\)00054-5](https://doi.org/10.1016/S0031-0182(96)00054-5)

465 Dobretsov, N.L., Polyansky, O.P., Reverdatto, V.V., Babichev, A.V., 2013. Dynamics of the Arctic  
466 and adjacent petroleum basins: a record of plume and rifting activity. *Russ. Geol.*  
467 *Geophys.* 54, 888-902. <https://doi.org/10.1016/j.rgg.2013.07.009>

468 Donnadiou, Y., Puceat, E., Moiroud, M., Guillocheau, F., Deconinck, J.F., 2016. A better-  
469 ventilated ocean triggered by Late Cretaceous changes in continental configuration. *Nat.*  
470 *Commun.* 7, 10316. <https://doi.org/10.1038/ncomms10316>

471 Evans, D., Sahoo, N., Renema, W., Cotton, L.J., Müller, W., Todd, J.A., Saraswati, P.K., Stassen,  
472 P., Ziegler, M., Pearson, P.N., Valdes, P.J., Affek, H.P., 2018. Eocene greenhouse climate  
473 revealed by coupled clumped isotope-Mg/Ca thermometry. *Proc. Natl. Acad. Sci. U.S.A.*  
474 115, 1174-1179. <https://doi.org/10.1073/pnas.1714744115>

475 Fiebig, J., Hofmann, S., Niklas, L., Lüdecke, T., Methner, K., Wacker, U., 2016. Slight pressure  
476 imbalances can affect accuracy and precision of dual inlet-based clumped isotope  
477 analysis. *Isotopes Environ. Health Stud.* 52, 12-28.  
478 <https://doi.org/10.1080/10256016.2015.1010531>

479 Frakes, L.A., 1979. *Climates throughout geologic time*. Elsevier, Amsterdam.

480 Frakes, L.A., Francis, J.E., 1988. A guide to Phanerozoic cold polar climates from high-latitude  
481 ice-rafting in the Cretaceous. *Nature* 333, 547-549. <https://doi.org/10.1038/333547a0>

482 Ghosh, P., Adkins, J., Affek, H., Balta, B., Guo, W., Schauble, E.A., Schrag, D., Eiler, J.M., 2006.  
483  $^{13}\text{C}$ – $^{18}\text{O}$  bonds in carbonate minerals: A new kind of paleothermometer. *Geochim.*  
484 *Cosmochim. Acta* 70, 1439-1456. <https://doi.org/10.1016/j.gca.2005.11.014>

485 Gradstein, F.M., Ogg, J.G., Schmitz, M.D., Ogg, G.M., 2012. *The Geologic Time Scale 2012*.  
486 Elsevier, p. 1176.

487 Grasby, S.E., McCune, G.E., Beauchamp, B., Galloway, J.M., 2017. Lower Cretaceous cold snaps  
488 led to widespread glendonite occurrences in the Sverdrup Basin, Canadian High Arctic.  
489 *Geol. Soc. Am. Bull.* 129, 771-787. <https://doi.org/10.1130/B31600.1>

490 Hemingway, J.E., Riddler, G.P., 1982. Basin inversion in North Yorkshire. *T. I. Min. Metall. B* 91,  
491 B175-B186.

492 Henkes, G.A., Passey, B.H., Wanamaker, A.D., Grossman, E.L., Ambrose, W.G., Carroll, M.L.,  
493 2013. Carbonate clumped isotope compositions of modern marine mollusk and  
494 brachiopod shells. *Geochim. Cosmochim. Acta* 106, 307-325.  
495 <https://doi.org/10.1016/j.gca.2012.12.020>

496 Henkes, G.A., Passey, B.H., Grossman, E.L., Shenton, B.J., Yancey, T.E., Pérez-Huerta, A., 2018.  
497 Temperature evolution and the oxygen isotope composition of Phanerozoic oceans from  
498 carbonate clumped isotope thermometry. *Earth Planet. Sci. Lett.* 490, 40-50.  
499 <https://doi.org/10.1016/j.epsl.2018.02.001>

500 Holland, H.D., 2004. The geologic history of seawater, in: Elderfield, H., Holland, H.D., Turekian,  
501 K.K. (Eds.), *Treatise on Geochemistry*, Vol. 6. The Oceans and Marine Geochemistry.  
502 Elsevier Pergamon, Kidlington, Oxford, pp. 583–625.

503 Holliday, D.W., 1999. Palaeotemperatures, thermal modelling and depth of burial studies in  
504 northern and eastern England. *Proc. Yorkshire Geol. Soc.* 52, 337-352.  
505 <https://doi.org/10.1144/pygs.52.4.337>

506 Huber, B.T., Hodell, D.A., Hamilton, C.P., 1995. Middle-Late Cretaceous climate of the southern  
507 high latitudes: Stable isotopic evidence for minimal equator-to-pole thermal gradients.  
508 *Geol. Soc. Am. Bull.* 107, 1164-1191. [https://doi.org/10.1130/0016-](https://doi.org/10.1130/0016-7606(1995)107<1164:MLCCOT>2.3.CO;2)  
509 [7606\(1995\)107<1164:MLCCOT>2.3.CO;2](https://doi.org/10.1130/0016-7606(1995)107<1164:MLCCOT>2.3.CO;2)

510 Huber, B.T., MacLeod, K.G., Watkins, D.K., Coffin, M.F., 2018. The rise and fall of the Cretaceous  
511 hot greenhouse climate. *Glob. Planet. Change* 167, 1-23.  
512 <https://doi.org/10.1016/j.gloplacha.2018.04.004>

513 Hurum, J.H., Milan, J., Hammer, O., Midtkandal, I., Amundsen, H., Saether, B., 2006. Tracking  
514 polar dinosaurs - new finds from the Lower Cretaceous of Svalbard. *Norw. J. Geol.* 86,  
515 397-402.

516 Jacobs, D.K., Sahagian, D.L., 1993. Climate-induced fluctuations in sea level during non-glacial  
517 times. *Nature* 361, 710-712. <https://doi.org/10.1038/361710a0>

518 Jaffrés, J.B.D., Shields, G.A., Wallmann, K., 2007. The oxygen isotope evolution of seawater: A  
519 critical review of a long-standing controversy and an improved geological water cycle  
520 model for the past 3.4 billion years. *Earth-Sci. Rev.* 83, 83-122.  
521 <https://doi.org/10.1016/j.earscirev.2007.04.002>

522 Janssen, N.M.M., 2003. Mediterranean Neocomian belemnites, part 2: The Berriasian-  
523 Valanginian boundary in southeast Spain (Río Argos, Cañada Lengua and Tornajo). *Scr.*  
524 *Geol.* 126, 121-183.

525 Jenkyns, H.C., Forster, A., Schouten, S., Sinninghe Damsté, J.S., 2004. High temperatures in the  
526 late Cretaceous Arctic Ocean. *Nature* 432, 888-892. <https://doi.org/10.1038/nature03143>

527 Jenkyns, H.C., Schouten-Huibers, L., Schouten, S., Sinninghe Damsté, J.S., 2012. Warm Middle  
528 Jurassic–Early Cretaceous high-latitude sea-surface temperatures from the Southern  
529 Ocean. *Clim. Past* 8, 215-226. <https://doi.org/10.5194/cp-8-215-2012>

530 Kelson, J.R., Huntington, K.W., Schauer, A.J., Saenger, C., Lechler, A.R., 2017. Toward a universal  
531 carbonate clumped isotope calibration: Diverse synthesis and preparatory methods  
532 suggest a single temperature relationship. *Geochim. Cosmochim. Acta* 197, 104-131.  
533 <https://doi.org/10.1016/j.gca.2016.10.010>

534 Kim, S.-T., O'Neil, J.R., 1997. Equilibrium and nonequilibrium oxygen isotope effects in synthetic  
535 carbonates. *Geochim. Cosmochim. Acta* 61, 3461-3475. [https://doi.org/10.1016/S0016-](https://doi.org/10.1016/S0016-7037(97)00169-5)  
536 [7037\(97\)00169-5](https://doi.org/10.1016/S0016-7037(97)00169-5)

537 Kim, S.-T., Mucci, A., Taylor, B.E., 2007. Phosphoric acid fractionation factors for calcite and  
538 aragonite between 25 and 75 °C: Revisited. *Chem. Geol.* 246, 135-146.  
539 <https://doi.org/10.1016/j.chemgeo.2007.08.005>

540 Kim, J.-H., van der Meer, J., Schouten, S., Helmke, P., Willmott, V., Sangiorgi, F., Koç, N.,  
541 Hopmans, E.C., Damsté, J.S.S., 2010. New indices and calibrations derived from the  
542 distribution of crenarchaeal isoprenoid tetraether lipids: Implications for past sea surface  
543 temperature reconstructions. *Geochim. Cosmochim. Acta* 74, 4639-4654.  
544 <https://doi.org/10.1016/j.gca.2010.05.027>

545 Klett, T.R., Wandrey, C.J., Pitman, J.K., 2011. Geology and petroleum potential of the north and  
546 east margins of the Siberian Craton, north of the Arctic Circle. *Arct. Pet. Geol.* 35, 413-  
547 431. <https://doi.org/10.1144/M35.27>

548 Klug, C., Schweigert, G., Fuchs, D., Kruta, I., Tischlinger, H., 2016. Adaptations to squid-style  
549 high-speed swimming in Jurassic belemnitids. *Biol. Lett.* 12, 1-5.  
550 <https://doi.org/10.1098/rsbl.2015.0877>

551 Kump, L.R., Pollard, D., 2008. Amplification of Cretaceous warmth by biological cloud  
552 feedbacks. *Science* 320, 195. <https://doi.org/10.1126/science.1153883>

553 LeGrande, A.N., Schmidt, G.A., 2006. Global gridded data set of the oxygen isotopic  
554 composition in seawater. *Geophys. Res. Lett.* 33, 1-5.  
555 <https://doi.org/10.1029/2006gl026011>

556 Lindquist, S.J., 1999. The Timan-Pechora Basin province of northwest Arctic Russia; Domanik,  
557 Paleozoic total petroleum system. USGS Open-File Report 99-50, 1-24.  
558 <https://doi.org/10.3133/ofr9950G>

559 Littler, K., Robinson, S.A., Bown, P.R., Nederbragt, A.J., Pancost, R.D., 2011. High sea-surface  
560 temperatures during the Early Cretaceous Epoch. *Nat. Geosci.* 4, 169-172.  
561 <https://doi.org/10.1038/ngeo1081>

562 Locarnini, R.A., Mishonov, A.V., Antonov, J.I., Boyer, T.P., Garcia, H.E., Baranova, O.K., Zweng,  
563 M.M., Paver, C.R., Reagan, J.R., Johnson, D.R., Hamilton, M., Seidov, D., 2013. World  
564 Ocean Atlas 2013, Volume 1: Temperature.

565 Lunt, D.J., Farnsworth, A., Loptson, C., Foster, G.L., Markwick, P., Brien, C.L., Pancost, R.D.,  
566 Robinson, S.A., Wrobel, N., 2016. Palaeogeographic controls on climate and proxy  
567 interpretation. *Clim. Past* 12, 1181-1198. <https://doi.org/10.5194/cp-12-1181-2016>

568 Marshall, J.D., 1992. Climatic and oceanographic isotopic signals from the carbonate rock  
569 record and their preservation. *Geol. Mag.* 129, 143-160.  
570 <https://doi.org/10.1017/s0016756800008244>

571 McArthur, J.M., Mutterlose, J., Price, G.D., Rawson, P.F., Ruffell, A., Thirlwall, M.F., 2004.  
572 Belemnites of Valanginian, Hauterivian and Barremian age: Sr-isotope stratigraphy,



573 composition ( $^{87}\text{Sr}/^{86}\text{Sr}$ ,  $\delta^{13}\text{C}$ ,  $\delta^{18}\text{O}$ , Na, Sr, Mg), and palaeo-oceanography. *Palaeogeogr.*  
574 *Palaeoclimatol. Palaeoecol.* 202, 253-272. [https://doi.org/10.1016/s0031-0182\(03\)00638-](https://doi.org/10.1016/s0031-0182(03)00638-2)  
575 2

576 McArthur, J.M., Janssen, N.M.M., Reboulet, S., Leng, M.J., Thirlwall, M.F., van de Schootbrugge,  
577 B., 2007. Palaeotemperatures, polar ice-volume, and isotope stratigraphy (Mg/Ca,  $\delta^{18}\text{O}$ ,  
578  $\delta^{13}\text{C}$ ,  $^{87}\text{Sr}/^{86}\text{Sr}$ ): The Early Cretaceous (Berriasian, Valanginian, Hauterivian). *Palaeogeogr.*  
579 *Palaeoclimatol. Palaeoecol.* 248, 391-430. <https://doi.org/10.1016/j.palaeo.2006.12.015>

580 McConnaughey, T., 1989.  $^{13}\text{C}$  and  $^{18}\text{O}$  isotopic disequilibrium in biological carbonates: II. *In vitro*  
581 simulation of kinetic isotope effects. *Geochim. Cosmochim. Acta* 53, 163-171.  
582 [https://doi.org/10.1016/0016-7037\(89\)90283-4](https://doi.org/10.1016/0016-7037(89)90283-4)

583 Meyer, K.W., Petersen, S.V., Lohmann, K.C., Winkelstern, I.Z., 2018. Climate of the Late  
584 Cretaceous North American Gulf and Atlantic Coasts. *Cretac. Res.* 89, 160-173.  
585 <https://doi.org/10.1016/j.cretres.2018.03.017>

586 Miller, K.G., 2009. Broken greenhouse windows. *Nat. Geosci.* 2, 465-466.  
587 <https://doi.org/10.1038/ngeo563>

588 Muehlenbachs, K., Clayton, R.N., 1976. Oxygen isotope composition of the oceanic crust and its  
589 bearing on seawater. *J. Geophys. Res.* 81, 4365-4369.  
590 <https://doi.org/10.1029/JB081i023p04365>

591 Muehlenbachs, K., 1998. The oxygen isotopic composition of the oceans, sediments and the  
592 seafloor. *Chem. Geol.* 145, 263-273. [https://doi.org/10.1016/S0009-2541\(97\)00147-2](https://doi.org/10.1016/S0009-2541(97)00147-2)

593 Mutterlose, J., Malkoc, M., Schouten, S., Sinninghe Damsté, J.S., Forster, A., 2010.  $\text{TEX}_{86}$  and  
594 stable  $\delta^{18}\text{O}$  paleothermometry of early Cretaceous sediments: Implications for belemnite  
595 ecology and paleotemperature proxy application. *Earth Planet. Sci. Lett.* 298, 286–298.  
596 <https://doi.org/10.1016/j.epsl.2010.07.043>

597 Mutterlose, J., Malkoc, M., Schouten, S., Sinninghe Damsté, J.S., 2012. Reconstruction of  
598 vertical temperature gradients in past oceans — Proxy data from the Hauterivian–early  
599 Barremian (Early Cretaceous) of the Boreal Realm. *Palaeogeogr. Palaeoclimatol.*  
600 *Palaeoecol.* 363–364, 135–143. <https://doi.org/10.1016/j.palaeo.2012.09.006>

601 Naafs, B.D.A., Pancost, R.D., 2016. Sea-surface temperature evolution across Aptian Oceanic  
602 Anoxic Event 1a. *Geology* 44, 959–962. <https://doi.org/10.1130/g38575.1>

603 Nunn, E.V., Price, G.D., Gröcke, D.R., Baraboshkin, E.Y., Leng, M.J., Hart, M.B., 2010. The  
604 Valanginian positive carbon isotope event in Arctic Russia: Evidence from terrestrial and  
605 marine isotope records and implications for global carbon cycling. *Cretac. Res.* 31, 577–  
606 592. <https://doi.org/10.1016/j.cretres.2010.07.007>

607 O'Brien, C.L., Robinson, S.A., Pancost, R.D., Sinninghe Damsté, J.S., Schouten, S., Lunt, D.J.,  
608 Alsenz, H., Bornemann, A., Bottini, C., Brassell, S.C., Farnsworth, A., Forster, A., Huber,  
609 B.T., Inglis, G.N., Jenkyns, H.C., Linnert, C., Littler, K., Markwick, P., McAnena, A.,  
610 Mutterlose, J., Naafs, B.D.A., Püttmann, W., Sluijs, A., van Helmond, N.A.G.M., Vellekoop,  
611 J., Wagner, T., Wrobel, N.E., 2017. Cretaceous sea-surface temperature evolution:  
612 Constraints from TEX<sub>86</sub> and planktonic foraminiferal oxygen isotopes. *Earth-Sci. Rev.* 172,  
613 224–247. <https://doi.org/10.1016/j.earscirev.2017.07.012>

614 O'Connor, L.K., Robinson, S.A., Naafs, B.D.A., Jenkyns, H.C., Henson, S., Clarke, M., Pancost,  
615 R.D., 2019. Late Cretaceous temperature evolution of the southern high latitudes: a TEX<sub>86</sub>  
616 perspective. *Paleoceanography and Paleoclimatology* 34, 436–454.  
617 <https://doi.org/10.1029/2018pa003546>

618 Passey, B.H., Henkes, G.A., 2012. Carbonate clumped isotope bond reordering and  
619 geospeedometry. *Earth Planet. Sci. Lett.* 351–352, 223–236.  
620 <https://doi.org/10.1016/j.epsl.2012.07.021>

621 Pekar, S.F., DeConto, R.M., 2006. High-resolution ice-volume estimates for the early Miocene:  
622 Evidence for a dynamic ice sheet in Antarctica. *Palaeogeogr. Palaeoclimatol. Palaeoecol.*  
623 231, 101-109. <https://doi.org/10.1016/j.palaeo.2005.07.027>

624 Petersen, S.V., Schrag, D.P., 2015. Antarctic ice growth before and after the Eocene-Oligocene  
625 transition: New estimates from clumped isotope paleothermometry. *Paleoceanography*  
626 30, 1305-1317. <https://doi.org/10.1002/2014PA002769>

627 Petersen, S.V., Tabor, C.R., Lohmann, K.C., Poulsen, C.J., Meyer, K.W., Carpenter, S.J., Erickson,  
628 J.M., Matsunaga, K.K.S., Smith, S.Y., Sheldon, N.D., 2016. Temperature and salinity of the  
629 Late Cretaceous Western Interior Seaway. *Geology* 44, 903-906.  
630 <https://doi.org/10.1130/g38311.1>

631 Petersen, S.V., Defliese, W.F., Saenger, C., Daëron, M., Huntington, K.W., John, C.M., Kelson,  
632 J.R., Coleman, A.S., Kluge, T., Olack, G.A., Schauer, A.J., Bajnai, D., Bonifacie, M.,  
633 Breitenbach, S.F., Fiebig, J., Fernandez, A.B., Henkes, G.A., Hodell, D., Katz, A., Kele, S.,  
634 Lohmann, K.C., Passey, B.H., Peral, M.Y., Petrizzo, D.A., Rosenheim, B.E., Tripathi, A.,  
635 Venturelli, R., Young, E.D., Winkelstern, I.Z., 2019. Effects of improved <sup>17</sup>O correction on  
636 interlaboratory agreement in clumped isotope calibrations, estimates of mineral-specific  
637 offsets, and temperature dependence of acid digestion fractionation. *Geochem. Geophys.*  
638 *Geosyst.* 20, 3495-3519. <https://doi.org/10.1029/2018GC008127>

639 Poulsen, C.J., Pollard, D., White, T.S., 2007. General circulation model simulation of the  $\delta^{18}\text{O}$   
640 content of continental precipitation in the middle Cretaceous: A model-proxy  
641 comparison. *Geology* 35, 199-202. <https://doi.org/10.1130/G23343A.1>

642 Price, G.D., 1999. The evidence and implications of polar ice during the Mesozoic. *Earth-Sci.*  
643 *Rev.* 48, 183-210. [https://doi.org/10.1016/s0012-8252\(99\)00048-3](https://doi.org/10.1016/s0012-8252(99)00048-3)

644 Price, G.D., Ruffell, A.H., Jones, C.E., Kalin, R.M., Mutterlose, J., 2000. Isotopic evidence for  
645 temperature variation during the early Cretaceous (late Ryazanian-mid-Hauterivian). *J.*  
646 *Geol. Soc.* 157, 335-343. <https://doi.org/10.1144/jgs.157.2.335>

647 Price, G.D., Nunn, E.V., 2010. Valanginian isotope variation in glendonites and belemnites from  
648 Arctic Svalbard: Transient glacial temperatures during the Cretaceous greenhouse.  
649 *Geology* 38, 251-254. <https://doi.org/10.1130/g30593.1>

650 Price, G.D., Passey, B.H., 2013. Dynamic polar climates in a greenhouse world: Evidence from  
651 clumped isotope thermometry of Early Cretaceous belemnites. *Geology* 41, 923-926.  
652 <https://doi.org/10.1130/g34484.1>

653 Price, G.D., Hart, M.B., Wilby, P.R., Page, K.N., 2015. Isotopic analysis of Jurassic (Calloviaian)  
654 mollusks from the Christian Malford lagerstätte (UK): Implications for ocean water  
655 temperature estimates based on belemnoids. *Palaios* 30, 645-654.  
656 <https://doi.org/10.2110/palo.2014.106>

657 Price, G.D., Janssen, N.M.M., Martinez, M., Company, M., Vandeveld, J.H., Grimes, S.T., 2018.  
658 A high-resolution belemnite geochemical analysis of Early Cretaceous (Valanginian-  
659 Hauterivian) environmental and climatic perturbations. *Geochem. Geophys. Geosyst.* 19,  
660 3832-3843. <https://doi.org/10.1029/2018gc007676>

661 Pucéat, E., Lecuyer, C., Sheppard, S.M.F., Dromart, G., Reboulet, S., Grandjean, P., 2003.  
662 Thermal evolution of Cretaceous Tethyan marine waters inferred from oxygen isotope  
663 composition of fish tooth enamels. *Paleoceanography* 18, 1029.  
664 <https://doi.org/10.1029/2002pa000823>

665 Railsback, L.B., Anderson, T.F., Ackerly, S.C., Cisne, J.L., 1989. Paleoceanographic modeling of  
666 temperature-salinity profiles from stable isotopic data. *Paleoceanography* 4, 585-591.  
667 <https://doi.org/10.1029/PA004i005p00585>

668 Rawson, P.F., 1973. Lower Cretaceous (Ryazanian-Barremian) marine connections and  
669 cephalopod migrations between the Tethyan and Boreal Realms, in: Casey, R., Rawson,  
670 P.F. (Eds.), *The Boreal Lower Cretaceous*. Seel House Press, Liverpool, pp. 131-144.

671 Reboulet, S., Szives, O., Aguirre-Urreta, B., Barragán, R., Company, M., Frau, C., Kakabadze,  
672 M.V., Klein, J., Moreno-Bedmar, J.A., Lukeneder, A., Pictet, A., Ploch, I., Raisossadat, S.N.,  
673 Vašíček, Z., Baraboshkin, E.J., Mitta, V.V., 2018. Report on the 6th International Meeting  
674 of the IUGS Lower Cretaceous Ammonite Working Group, the Kilian Group (Vienna,  
675 Austria, 20th August 2017). *Cretac. Res.* 91, 100-110.  
676 <https://doi.org/10.1016/j.cretres.2018.05.008>

677 Reicherter, K., Wiedmann, J., Herbin, J.P., 1996. Distribution of organic-rich sediments in  
678 Subbetic sections during the Aptian-Turonian (Betic Cordillera, Southern Spain). *Rev. Soc.*  
679 *Geol. Esp.* 9, 75-88.

680 Rogov, M.A., Ershova, V.B., Shchepetova, E.V., Zakharov, V.A., Pokrovsky, B.G., Khudoley, A.K.,  
681 2017. Earliest Cretaceous (late Berriasian) glendonites from Northeast Siberia revise the  
682 timing of initiation of transient Early Cretaceous cooling in the high latitudes. *Cretac. Res.*  
683 71, 102-112. <https://doi.org/10.1016/j.cretres.2016.11.011>

684 Ryb, U., Eiler, J.M., 2018. Oxygen isotope composition of the Phanerozoic ocean and a possible  
685 solution to the dolomite problem. *Proc. Natl. Acad. Sci. U.S.A.* 115, 6602-6607.  
686 <https://doi.org/10.1073/pnas.1719681115>

687 Sælen, G., 1989. Diagenesis and construction of the belemnite rostrum. *Palaeontology* 32, 765-  
688 797.

689 Sagoo, N., Valdes, P., Flecker, R., Gregoire, L.J., 2013. The Early Eocene equable climate  
690 problem: Can perturbations of climate model parameters identify possible solutions?  
691 *Philos. T. R. Soc. A* 371, 20130123. <https://doi.org/10.1098/rsta.2013.0123>

692 Schmidt, G.A., Mysak, L.A., 1996. Can increased poleward oceanic heat flux explain the warm  
693 Cretaceous climate? *Paleoceanography* 11, 579-593. <https://doi.org/10.1029/96pa01851>

694 van de Schootbrugge, B., Föllmi, K.B., Bulot, L.G., Burns, S.J., 2000. Paleoceanographic changes  
695 during the early Cretaceous (Valanginian-Hauterivian): evidence from oxygen and carbon  
696 stable isotopes. *Earth Planet. Sci. Lett.* 181, 15-31. [https://doi.org/10.1016/S0012-](https://doi.org/10.1016/S0012-821X(00)00194-1)  
697 [821X\(00\)00194-1](https://doi.org/10.1016/S0012-821X(00)00194-1)

698 Scotese, C.R., 2014. Atlas of Early Cretaceous Paleogeographic Maps, PALEOMAP Atlas for  
699 ArcGIS, volume 2, The Cretaceous, Maps 23-31, Mollweide Projection, Evanston, IL, USA.

700 Shackleton, N.J., Kennett, J.P., 1975. Paleotemperature history of the Cenozoic and the  
701 initiation of antarctic glaciation: oxygen and carbon isotope analyses in DSDP sites 277,  
702 279, and 281. *Deep Sea Drilling Project Initial Reports* 29, 743-755.  
703 <https://doi.org/10.2973/dsdp.proc.29.117.1975>

704 Shulgina, N.I., Burdykina, M.D., Basov, V.A., Arhus, N., 1994. Distribution of ammonites,  
705 foraminifera and dinoflagellate cysts in the Lower Cretaceous reference sections of the  
706 Khatanga Basin, and Boreal Valanginian biogeography. *Cretac. Res.* 15, 1-16.  
707 <https://doi.org/10.1006/cres.1994.1001>

708 Słowakiewicz, M., Tucker, M.E., Vane, C.H., Harding, R., Collins, A., Pancost, R.D., 2015. Shale-  
709 gas potential of the mid-Carboniferous Bowland-Hodder Unit in the Cleveland Basin  
710 (Yorkshire), central Britain. *J. Pet. Geol.* 38, 59-75. <https://doi.org/10.1111/jpg.12598>

711 Spicer, R.A., Ahlberg, A., Herman, A.B., Hofmann, C.-C., Raikevich, M., Valdes, P.J., Markwick,  
712 P.J., 2008. The Late Cretaceous continental interior of Siberia: A challenge for climate  
713 models. *Earth Planet. Sci. Lett.* 267, 228-235. <https://doi.org/10.1016/j.epsl.2007.11.049>

714 Spicer, R.A., Herman, A.B., 2010. The Late Cretaceous environment of the Arctic: A quantitative  
715 reassessment based on plant fossils. *Palaeogeogr. Palaeoclimatol. Palaeoecol.* 295, 423-  
716 442. <https://doi.org/10.1016/j.palaeo.2010.02.025>

717 Stevens, K., Mutterlose, J., Schweigert, G., 2014. Belemnite ecology and the environment of the  
718 Nusplingen Plattenkalk (Late Jurassic, southern Germany): Evidence from stable isotope  
719 data. *Lethaia* 47, 512-523. <https://doi.org/10.1111/let.12076>

720 Super, J.R., Chin, K., Pagani, M., Li, H., Tabor, C., Harwood, D.M., Hull, P.M., 2018. Late  
721 Cretaceous climate in the Canadian Arctic: Multi-proxy constraints from Devon Island.  
722 *Palaeogeogr. Palaeoclimatol. Palaeoecol.* 504, 1-22.  
723 <https://doi.org/10.1016/j.palaeo.2018.03.004>

724 Tarduno, J.A., Brinkman, D.B., Renne, P.R., Cottrell, R.D., Scher, H., Castillo, P., 1998. Evidence  
725 for extreme climatic warmth from Late Cretaceous Arctic vertebrates. *Science* 282, 2241-  
726 2244. <https://doi.org/10.1126/science.282.5397.2241>

727 Tierney, J.E., Tingley, M.P., 2014. A Bayesian, spatially-varying calibration model for the TEX<sub>86</sub>  
728 proxy. *Geochim. Cosmochim. Acta* 127, 83-106.  
729 <https://doi.org/10.1016/j.gca.2013.11.026>

730 Upchurch, G.R., Kiehl, J., Shields, C., Scherer, J., Scotese, C., 2015. Latitudinal temperature  
731 gradients and high-latitude temperatures during the latest Cretaceous: Congruence of  
732 geologic data and climate models. *Geology* 43, 683-686.  
733 <https://doi.org/10.1130/g36802.1>

734 Veizer, J., 1974. Chemical diagenesis belemnite shells possible consequences for  
735 paleotemperature determinations. *Neues Jahrb. Geol. Palaontol. Abhand.* 147, 91-111.

736 Veizer, J., Prokoph, A., 2015. Temperatures and oxygen isotopic composition of Phanerozoic  
737 oceans. *Earth-Sci. Rev.* 146, 92-104. <https://doi.org/10.1016/j.earscirev.2015.03.008>

738 Vickers, M.L., Price, G.D., Jerrett, R.M., Watkinson, M., 2016. Stratigraphic and geochemical  
739 expression of Barremian–Aptian global climate change in Arctic Svalbard. *Geosphere* 12,  
740 1594-1605. <https://doi.org/10.1130/ges01344.1>

741 Vickers, M.L., Bajnai, D., Price, G.D., Linckens, J., Fiebig, J., 2019. Southern high latitude warmth  
742 during Jurassic–Cretaceous: New evidence from clumped isotope thermometry. *Geology*  
743 47, 724-728. <https://doi.org/10.1130/G46263.1>

744 Voigt, S., Wilmsen, M., Mortimore, R.N., Voigt, T., 2003. Cenomanian palaeotemperatures  
745 derived from the oxygen isotopic composition of brachiopods and belemnites: evaluation  
746 of Cretaceous palaeotemperature proxies. *Int. J. Earth Sci.* 92, 285-299.  
747 <https://doi.org/10.1007/s00531-003-0315-1>

748 Wacker, U., Fiebig, J., Tödter, J., Schöne, B.R., Bahr, A., Friedrich, O., Tütken, T., Gischler, E.,  
749 Joachimski, M.M., 2014. Empirical calibration of the clumped isotope paleothermometer  
750 using calcites of various origins. *Geochim. Cosmochim. Acta* 141, 127-144.  
751 <https://doi.org/10.1016/j.gca.2014.06.004>

752 Wallmann, K., 2004. Impact of atmospheric CO<sub>2</sub> and galactic cosmic radiation on Phanerozoic  
753 climate change and the marine  $\delta^{18}\text{O}$  record. *Geochem. Geophys. Geosyst.* 5, 1-29.  
754 <https://doi.org/10.1029/2003gc000683>

755 Wang, Y., Huang, C., Sun, B., Quan, C., Wu, J., Lin, Z., 2014. Paleo-CO<sub>2</sub> variation trends and the  
756 Cretaceous greenhouse climate. *Earth-Sci. Rev.* 129, 136-147.  
757 <https://doi.org/10.1016/j.earscirev.2013.11.001>

758 White, T., Gonzalez, L., Ludvigson, G., Poulsen, C., 2001. Middle Cretaceous greenhouse  
759 hydrologic cycle of North America. *Geology* 29, 363-366. [https://doi.org/10.1130/0091-  
760 7613\(2001\)029<0363:Mcghco>2.0.Co;2](https://doi.org/10.1130/0091-7613(2001)029<0363:Mcghco>2.0.Co;2)

761 Wierzbowski, H., Rogov, M.A., Matyja, B.A., Kiselev, D., Ippolitov, A., 2013. Middle–Upper  
762 Jurassic (Upper Callovian–Lower Kimmeridgian) stable isotope and elemental records of  
763 the Russian Platform: Indices of oceanographic and climatic changes. *Glob. Planet.*  
764 *Change* 107, 196-212. <https://doi.org/10.1016/j.gloplacha.2013.05.011>



765 Wierzbowski, H., Bajnai, D., Wacker, U., Rogov, M.A., Fiebig, J., Tesakova, E.M., 2018. Clumped  
766 isotope record of salinity variations in the Subboreal Province at the middle–late Jurassic  
767 transition. *Glob. Planet. Change* 167, 172-189.  
768 <https://doi.org/10.1016/j.gloplacha.2018.05.014>

769 Witkowski, C.R., Weijers, J.W.H., Blais, B., Schouten, S., Sinninghe Damsté, J.S., 2018. Molecular  
770 fossils from phytoplankton reveal secular  $p\text{CO}_2$  trend over the Phanerozoic. *Sci. Adv.* 4,  
771 eaat4556. <https://doi.org/10.1126/sciadv.aat4556>

772 Young, A., Flament, N., Maloney, K., Williams, S., Matthews, K., Zahirovic, S., Müller, R.D., 2019.  
773 Global kinematics of tectonic plates and subduction zones since the late Paleozoic Era.  
774 *Geosci. Front.* 10, 989-1013. <https://doi.org/10.1016/j.gsf.2018.05.011>

775 Zakharov, V.A., Bogomolov, Y.I., Il'ina, V.I., Konstantinov, A.G., Kurushin, N.I., Lebedeva, N.K.,  
776 Meledina, S.V., Nikitenko, B.L., Sobolev, E.S., Shurygin, B.N., 1997. Boreal zonal standard  
777 and biostratigraphy of the Siberian Mesozoic. *Russ. Geol. Geophys.* 38, 965-993.

778 Zeebe, R.E., 1999. An explanation of the effect of seawater carbonate concentration on  
779 foraminiferal oxygen isotopes. *Geochim. Cosmochim. Acta* 63, 2001-2007.  
780 [https://doi.org/10.1016/S0016-7037\(99\)00091-5](https://doi.org/10.1016/S0016-7037(99)00091-5)

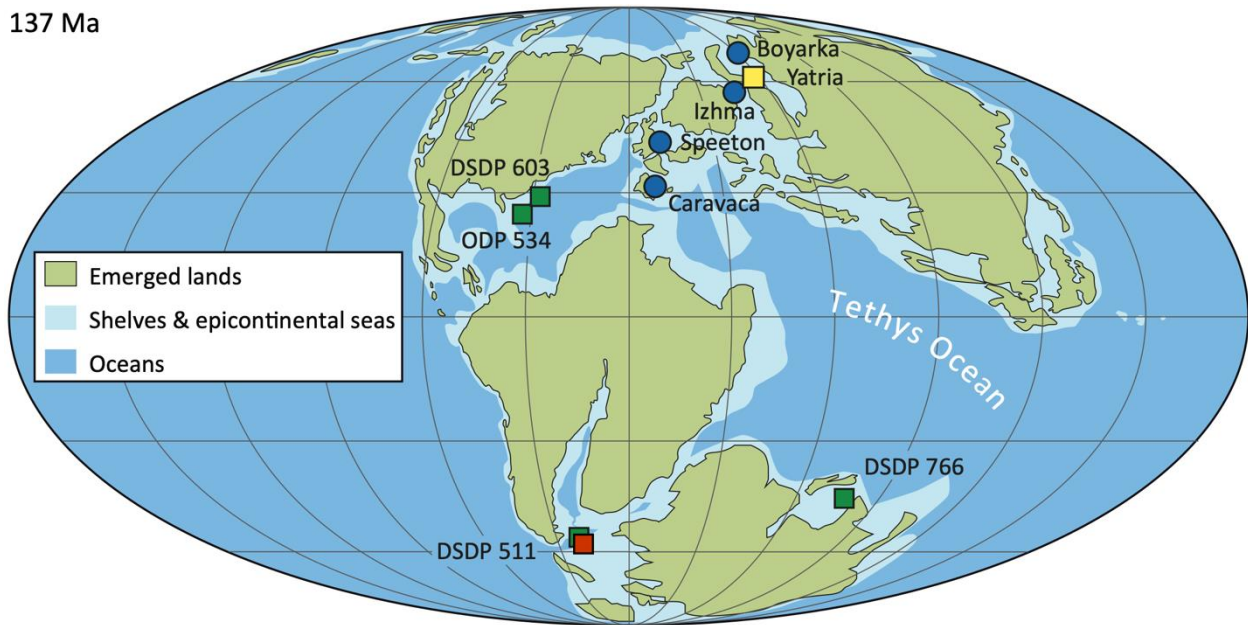
781 Zeebe, R.E., 2001. Seawater pH and isotopic paleotemperatures of Cretaceous ocean.  
782 *Palaeogeogr. Palaeoclimatol. Palaeoecol.* 170, 49-57. [https://doi.org/10.1016/S0031-](https://doi.org/10.1016/S0031-0182(01)00226-7)  
783 [0182\(01\)00226-7](https://doi.org/10.1016/S0031-0182(01)00226-7)

784 Zhou, J., Poulsen, C.J., Pollard, D., White, T.S., 2008. Simulation of modern and middle  
785 Cretaceous marine  $\delta^{18}\text{O}$  with an ocean-atmosphere general circulation model.  
786 *Paleoceanography* 23, PA3223. <https://doi.org/10.1029/2008pa001596>

787 Zhu, J., Poulsen, C.J., Tierney, J.E., 2019. Simulation of Eocene extreme warmth and high climate  
788 sensitivity through cloud feedbacks. *Sci. Adv.* 5, eaax1874.  
789 <https://doi.org/10.1126/sciadv.aax1874>

791 **Figures**

137 Ma

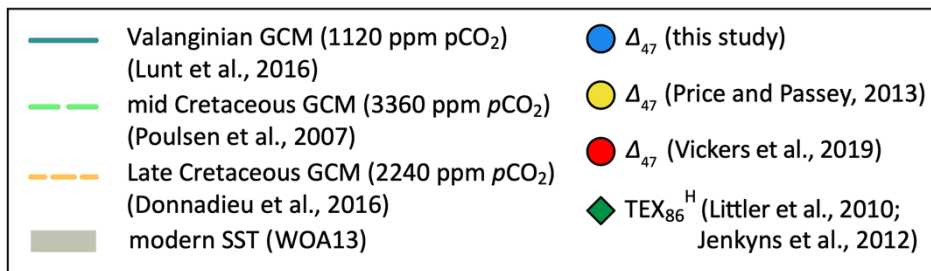
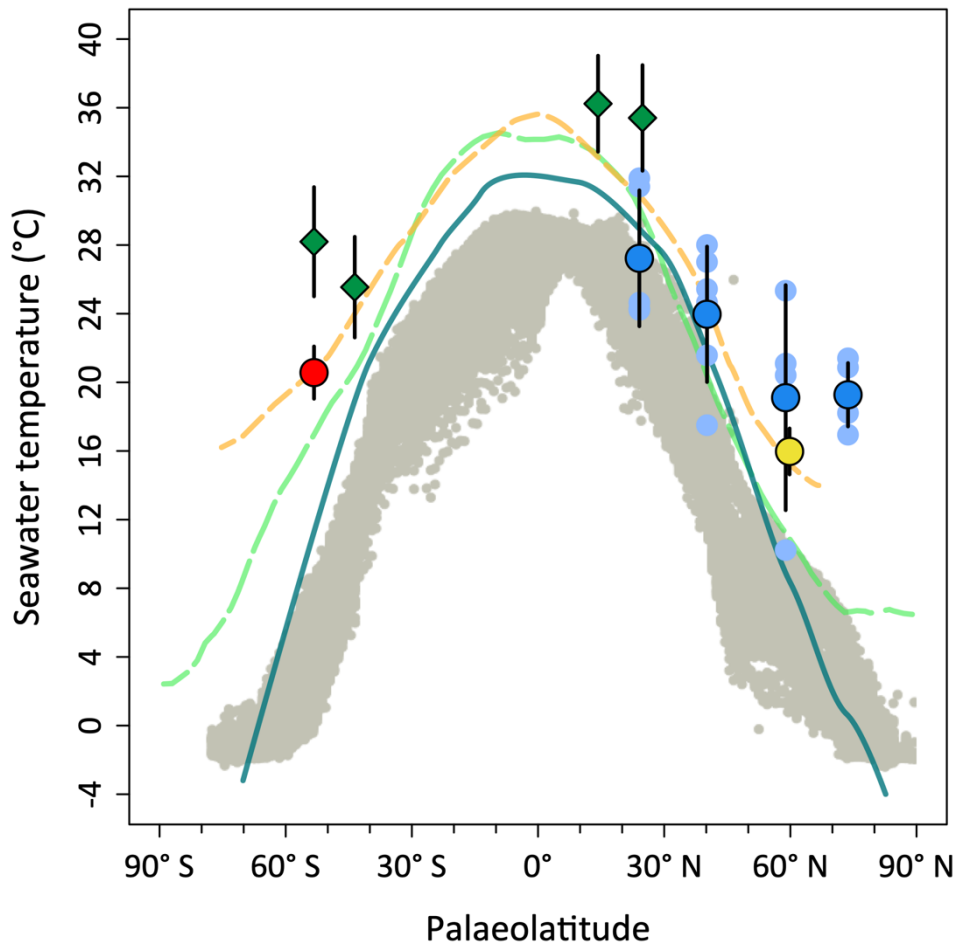


792  
793 **Fig. 1.** Early Cretaceous palaeogeographic reconstruction with locations of the discussed study  
794 sites. Map modified after Scotese (2014). Blue circles = data from this study; green squares =  
795 location of published Early Cretaceous TEX<sub>86</sub> data (Littler et al. 2011; Jenkyns et al. 2012). The  
796 locations of additional published  $\Delta_{47}$ -based temperature data are marked with a yellow square  
797 (Price and Passey, 2013) and a red square (Vickers et al. 2019). The palaeolatitude estimates are  
798 consistent with Young et al. (2019) that are used for Figs 3 and 4.

		Tethyan ammonite zonation	Sub-Boreal ammonite zonation	Boreal (Siberian) ammonite zonation	
Valanginian	Upper	Criosarasinella furcillata	Endemoceras amblygonium	Homolsomites bojarkensis	
			Eleniceras paucinodum	Dichotomites bidichotomus	Neocraspedites kotschetkovi
			Stolcoceras tuberculatum		Dichotomites bidichotomus
		Neocomites peregrinus	Dichotomites		Polyptychites triplodiptychus
			Saynoceras verrucosum		Prodichotomites
	Lower	Karakaschiceras inostranzewi		Polyptychites michalskii	
		Neocomites neocomiensiformis	Polyptychites		
		Tirnovella pertransiens	Platylenticeras	Astieriptychites astieriptychus	
	Peregrinoceras albidum		Polyptychites quadrifidus		
	Berriasian	Upper	Tirnovella apillensis	Surites stenomphalus	Neotollia klimovskiensis
Tollia tolli					

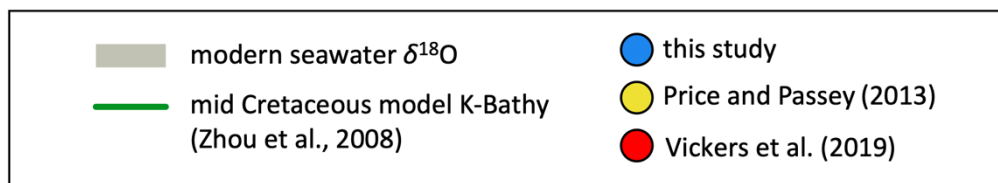
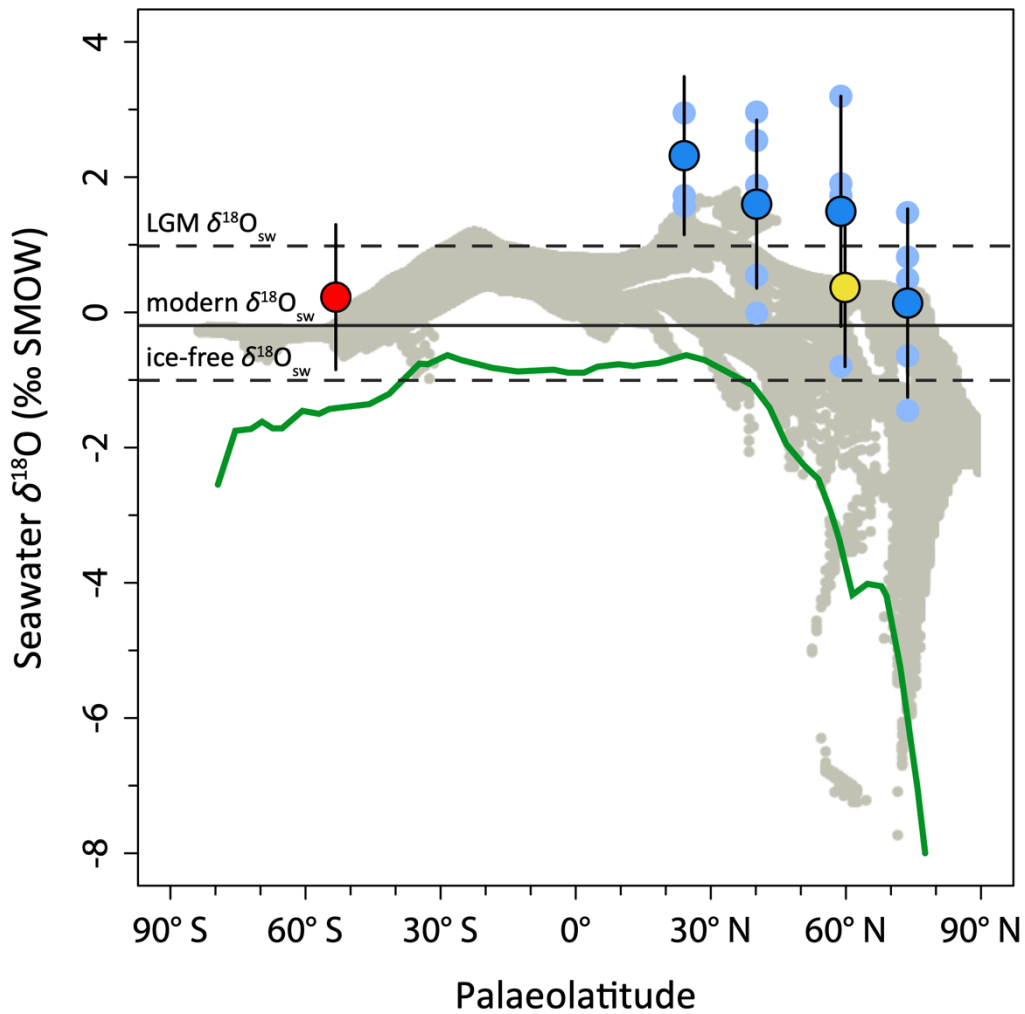
Zonal range of data from the Yatria River

799 **Fig. 2.** Biostratigraphic correlation of the Early Cretaceous Tethyan (Reboulet et al., 2018) sub-  
800 Boreal and Boreal (Gradstein et al. 2012; Nunn et al. 2010; Shulgina et al., 1994; Zakharov et al.,  
801 1997; Baraboshkin, 2004) ammonite schemes. The green shaded area indicates the position of  
802 sampled Valanginian zones for Tethyan (Caravaca, Spain), Sub-Boreal (Speeton), and Boreal  
803 sites (Khatanga Basin and Pechora Basin). The ammonite range of additional Valanginian  $\Delta_{47}$   
804 data from the Yatria River is shown (Price and Passey 2013). Early Cretaceous southern high  
805 latitude data shown on Figs 3 and 4 have less constrained biostratigraphy (Vickers et al., 2019).



806 **Fig. 3.** Early Cretaceous (Valanginian) meridional temperature reconstruction. Mean annual  
 807 surface temperature observations from the World Ocean Atlas (Locarnini et al., 2013).  
 808 Valanginian TEX<sub>86</sub> temperatures (Littler et al., 2011) were recalculated using the TEX<sub>86</sub><sup>H</sup>  
 809 calibration (Kim et al., 2010). Dark blue circles show mean Δ<sub>47</sub>-based temperatures from this  
 810 study with ± uncertainties corresponding to the standard deviation from individual belemnites  
 811 (light blue circles). Additional Δ<sub>47</sub> data of Vickers et al., (2019) (for the Early Cretaceous) and  
 812 Price and Passey (2013) (Valanginian) were converted to temperatures using the synthetic  
 813 calcite calibration of Petersen et al. (2019). Early Cretaceous data are compared with sea  
 814 surface temperatures from the Early Cretaceous (Valanginian) GCM with 4x pre-industrial pCO<sub>2</sub>

815 (Lunt et al., 2016) a mid-Cretaceous GCM with 12x pre-industrial  $p\text{CO}_2$  (Poulsen et al., 2007) and  
816 a Late Cretaceous GCM with 8x pre-industrial  $p\text{CO}_2$  (Donnadieu et al., 2016). Thermal gradients  
817 of the simulations have been calculated from an average over the longitudes including the  
818 South Atlantic sector and the Tethyan area (see Donnadieu et al., 2016). A version of this plot  
819 where  $\Delta_{47}$ -based temperatures are calculated using the Wacker et al. (2014) equation is shown  
820 in the Supplementary Information.



821 **Fig. 4.** Early Cretaceous (Valanginian) meridional seawater oxygen isotope gradient. Modern  
 822 gridded mean annual  $\delta^{18}\text{O}_{\text{sw}}$  values from LeGrande and Schmidt (2006).  $\delta^{18}\text{O}_{\text{sw}}$  (‰ SMOW)  
 823 calculated using the Kim and O'Neil (1997) equation (see Supplementary Figure 2 for Coplen  
 824 (2007) equation) with additional Valanginian data derived from Price and Passey (2013) and  
 825 Vickers et al. (2019). Dark blue circles are mean estimates and  $\pm$  uncertainties are standard  
 826 deviations. Light blue circles are estimates from individual belemnites. Modelled mid  
 827 Cretaceous mean annual zonal average of  $\delta^{18}\text{O}_{\text{sw}}$  after Zhou, et al. (2008).

828 **Table 1.** Clumped and bulk isotopic composition of Early Cretaceous belemnites

Sample	Taxonomy	Location	N	$\delta^{13}\text{C}$ (‰ VPDB)	$\delta^{18}\text{O}$ (‰ VPDB)	$\Delta_{47}$ (RFAC) (‰)	Temperature (°C)	$\delta^{18}\text{O}_{\text{sw}}$ (‰ SMOW) Coplen (2007)	$\delta^{18}\text{O}_{\text{sw}}$ (‰ SMOW) Kim and O'Neil (1997)
KH18-10.50	<i>Acroteuthis</i> sp.	Boyarka	5	0.22	-1.55	0.707 (±0.005)	19 (±1)	-2.1 (±0.3)	-0.6 (±0.3)
KH18-11.20	indet.	Boyarka	5	1.12	-0.48	0.701 (±0.006)	21 (±2)	-0.6 (±0.4)	0.8 (±0.4)
KH18-27.00	<i>Lagonibelus</i> sp.	Boyarka	6	0.96	0.03	0.713 (±0.006)	17 (±2)	-0.9 (±0.4)	0.5 (±0.4)
KH18-2.85	indet.	Boyarka	5	0.38	0.07	0.699 (±0.009)	21 (±3)	0.0 (±0.6)	1.5 (±0.6)
KH18-7.10	<i>Pachyteuthis</i> sp.	Boyarka	5	0.60	-2.19	0.709 (±0.007)	18 (±2)	-2.9 (±0.5)	-1.5 (±0.5)
YCL214-031	<i>Berriasibelus</i> sp.	Caravaca	6	-1.25	-0.57	0.670 (±0.012)	32 (±5)	1.4 (±0.9)	2.9 (±0.9)
YG14-015	<i>Duvalia</i> sp.	Caravaca	3	0.50	0.37	0.671 (±0.007)	31 (±3)	2.3 (±0.5)	3.8 (±0.5)
YP14-005	<i>Hibolithes</i> sp.	Caravaca	5	1.74	-0.41	0.691 (±0.013)	24 (±4)	0.1 (±0.9)	1.6 (±0.9)
YP14-001	<i>Duvalia</i> cf. <i>lata</i>	Caravaca	6	-0.29	-0.50	0.690 (±0.009)	25 (±3)	0.1 (±0.6)	1.6 (±0.7)
YP14-014	<i>Duvalia</i> <i>binervia</i>	Caravaca	4	0.95	-0.27	0.691 (±0.009)	24 (±3)	0.3 (±0.6)	1.7 (±0.6)
PC7-B1	<i>Pachyteuthis</i> sp.	Izhma	7	-0.49	0.21	0.735 (±0.004)	10 (±1)	-2.1 (±0.3)	-0.8 (±0.3)
PC7-B2	<i>Pachyteuthis</i> sp.	Izhma	6	0.19	0.56	0.700 (±0.003)	21 (±1)	0.5 (±0.2)	1.9 (±0.2)

PC9-G23	indet.	Izhma	5	-0.79	0.52	0.702 (±0.007)	20 (±2)	0.3 (±0.5)	1.7 (±0.5)
PC9-G8	<i>Acroteuthis</i> sp.	Izhma	7	1.16	0.98	0.688 (±0.005)	25 (±2)	1.7 (±0.3)	3.2 (±0.3)
D2E	<i>Acroteuthis</i> sp.	Speeton	2	-0.46	-0.36	0.690 (±0.007)	25 (±2)	0.3 (±0.5)	1.7 (±0.5)
D3D	<i>Acroteuthis</i> sp.	Speeton	2	-0.09	-0.21	0.680 (±0.020)	28 (±7)	1.1 (±1.4)	2.5 (±1.4)
D4A	<i>Acroteuthis</i> sp.	Speeton	6	0.51	0.41	0.683 (±0.004)	27 (±1)	1.5 (±0.3)	3.0 (±0.3)
SP 1181	<i>Acroteuthis</i> sp.	Speeton	5	-0.12	-0.60	0.711 (±0.004)	18 (±1)	-1.4 (±0.3)	0.0 (±0.3)
SP 1297	<i>Acroteuthis</i> sp.	Speeton	4	0.60	-0.89	0.699 (±0.005)	22 (±2)	-0.9 (±0.3)	0.5 (±0.3)
SP 1S22C	<i>Acroteuthis</i> sp.	Speeton	5	0.60	-0.36	0.688 (±0.005)	25 (±2)	0.4 (±0.3)	1.9 (±0.3)

829 The standard error of the carbonate  $\delta^{13}\text{C}$  and  $\delta^{18}\text{O}$  values is 0.01‰. The  $\pm$  uncertainty in the  
830  $\Delta_{47}$  (RFAC) values represents the (external) standard error of 2–7 replicate analyses, multiplied by  
831 the  $t$ -value that corresponds to the number of replicates (68.2% confidence interval). The  
832  $\Delta_{47}$  (RFAC) values were converted to temperatures using synthetic calcite calibration (Petersen et  
833 al., 2019) as discussed in the text (Data S1). The error in the calculated temperatures and  $\delta^{18}\text{O}_{\text{sw}}$   
834 correspond to the standard error of the  $\Delta_{47}$  (RFAC) values.



835 **Table 2.** Mean seawater temperatures and  $\delta^{18}\text{O}_{\text{sw}}$  for the locations in this study.

Location	Palaeolatitude	Number of belemnites	Mean seawater temperature (°C)	Mean $\delta^{18}\text{O}_{\text{sw}}$ (‰ SMOW) Coplen (2007)	Mean $\delta^{18}\text{O}_{\text{sw}}$ (‰ SMOW) Kim and O'Neil (1997)
Caravaca	24° N	5	27 (±4)	0.8 (±1.1)	2.3 (±1.2)
Speeton	40° N	6	24 (±4)	0.1 (±1.2)	1.6 (±1.2)
Izhma	59° N	4	19 (±7)	0.1 (±1.7)	1.5 (±1.7)
Boyarka	74° N	5	19 (±2)	-1.3 (±1.4)	0.1 (±1.4)

836 The ± uncertainties for the mean temperatures are calculated using the standard deviation of  
 837 the  $\Delta_{47}(\text{RFAC})$  values of the individual belemnites (Table 1). This uncertainty was combined with  
 838 the standard deviation of the  $\delta^{18}\text{O}$  values of the individual belemnites to calculate the ±  
 839 uncertainties for the mean  $\delta^{18}\text{O}_{\text{sw}}$  values. Palaeolatitude estimates are from Young et al. (2019).